PEG-co-PCL nanoparticles modified with MMP-2/9 activatable low molecular weight protamine for enhanced targeted glioblastoma therapy

Guangzhi Gu [a,1], Huimin Xia [a,c,1], Quanyin Hu [a], Zhongyang Liu [a], Mengyin Jiang [d], Ting Kang [a], Deyu Miao [d], Yifan Tu [a], Zhiqing Pang [a], Qingxiang Song [b], Lei Yao [b], Hongzhan Chen [b], Xiaoling Gao [b,*], Jun Chen [a,*]

[a] Key Laboratory of Smart Drug Delivery, Ministry of Education & PLA, School of Pharmacy, Fudan University, Lane 826, Zhangheng Road, Shanghai 201203, PR China
[b] Department of Pharmacology, Institute of Medical Sciences, Shanghai Jiaotong University School of Medicine, 280 South Chongqing Road, Shanghai 200025, PR China
[c] Shanghai Institute for Food and Drug Control (SIFDC), Lane 1500, Zhangheng Road, Shanghai 201203, PR China
[d] School of Pharmacy, Shandong University of Traditional Chinese Medicine, Jinan, Shandong, PR China

ARTICLE INFO

ABSTRACT

By taking advantage of the dramatically upregulated expression of matrix metalloproteinases MMP-2 and MMP-9 in glioblastomas and the powerful transport ability of low molecular weight protamine (LMWP), we constructed an activatable low molecular weight protamine (ALMWP) and conjugated it to PEG-PCL nanoparticles (NP) to develop a 'smart' drug delivery system for enhanced targeted glioblastoma therapy. Important parameters such as particle size distribution, zeta potential and surface content were determined, which confirmed the conjugation of ALMWP to the surface of nanoparticle. ALMWP-NP loaded with paclitaxel (PTX) exhibited a desirable pharmacokinetic and biodistribution profiles for anti-glioblastoma drug delivery. Cellular experiments showed that ALMWP-NP exhibited significantly elevated MMP-dependent cellular accumulation in C6 cells via lipid raft-mediated endocytosis and energy-dependent macropinocytosis, and improved the cytotoxicity of PTX. In vitro C6 tumor spheroid uptake confirmed the tumor penetrating ability of ALMWP-NP, in vivo imaging and glioma distribution justified its specific accumulation in the glioma. The improved glioma-targeting and tumor penetration led to an anticipated enhanced in vivo anti-glioblastoma effect: animals (nude mice bearing intracranial C6 glioma) treated with ALMWP-NP-PTX survive significantly longer than those treated with saline, Taxol® NP-PTX and LMWP-NP-PTX. The findings here offered strong evidence for the glioblastoma-targeting therapy of ALMWP-NP-PTX, and could also lead to a significant advancement in the application of CPPs for targeted therapy of glioma.

1. Introduction

Glioblastoma multiforme (GBM), known as grade IV glioma, is the most common and malignant form of brain tumors, accounting for approximately 40% of all primary brain tumors and 70% of all malignant gliomas [1]. Treatment of glioblastoma represents one of the most formidable challenges in oncology due to the poor cellular differentiation, invasiveness of glioblastoma and its surgical inaccessibility to complete resection [2]. Chemotherapy seems essential in the auxiliary treatment of glioblastoma, but results have been modest thus far due to the existence of blood–brain barrier (BBB) and blood–brain tumor barrier (BTB) [3,4].

In recent years, tremendous attention and effort have been focused on the development of active targeting drug delivery systems (DDS), in particular, biodegradable polymeric nanoparticles, to circumvent the BBB/BTB and elevate drug delivery to glioblastomas [5]. Numerous physicochemical properties of nanoparticles make them ideal devices for the delivery of therapeutic agents to glioblastomas [6]. As shown by a number of reports, surface modification of the nanoparticles with specific targeting ligands enables their entry into gliomas after intravenous administration via receptor-mediated pathways [7]. However, receptor-mediated endocytosis is a saturated pathway, which restricts the amount of nanoparticles that are available for cellular uptake [8]. What's more, receptor-mediated endocytosis of nanoparticles usually leads to lysosomal delivery and subsequent considerably high degradation [9]. Nanocarriers that are able to avoid this would be of interest.

The past decade has witnessed an escalating interest in the therapeutic applications of cell penetrating peptides (CPPs). CPPs

* Corresponding authors. Tel.: +86 21 51980066.
  E-mail addresses: shellygao1@yahoo.com.cn (X. Gao), chenjun@fudan.edu.cn, chenjun_1974@yahoo.com.cn (J. Chen).
[1] Authors contributed equally.

are typically short cationic peptides that are rapidly internalized across cell membranes [10]. A large variety of cargoes such as small molecules, proteins, peptides, fragments of DNA, liposomes and nanoparticles, have been effectively delivered into cells via CPPs, independent of a membrane receptor [9]. Among the CPPs, low molecular weight protamine (LMWP) has attracted growing interest as it possesses similar potency as TAT in mediating cellular translocation of its payloads, and can be produced in mass quantities direct from native protamine, while others must be chemically synthesized [11,12]. Furthermore, unlike other cationic peptides, it was proved to be non-toxic [13,14]. Despite these advantages, just as in the case of other CPPs, it is hardly optimal to apply LMWP-functionalized DDS for systemic administration, due to its lack of selectivity in cellular association and tissue biodistribution, which could increase the risk of drug-induced toxic effect on normal tissues [9].

Development of protease-sensitive DDS by exploiting the increased protease expression at the tumor sites is an area of drug development showing great promise [15]. A strategy termed activatable cell penetrating peptides (ACPP) has been developed by Tisen's group [16,17]. The reported ACCP contain a sequence of polycationic CPP, a matrix metalloproteinases (MMP)-sensitive peptide linker and a polyanionic inhibitory domain. In the MMP rich tumor environment, the linker is selectively cleaved and the inhibitory acidic peptide dissociates based on its off-rate, thereby exposing the cationic CPP to deliver its linked cargo into the surrounding tumor cells. This ACPP approach has shed light on the resolution of CPP-mediated drug delivery dilemma. Recent insight into the fundamental processes governing glioma angiogenesis and invasion demonstrated that 72-kDa gelatinase-A (MMP-2) and 92-kDa gelatinase-B (MMP-9) together play an important role in the invasiveness of glioblastomas, mediating the degradation of the extracellular matrix (ECM) and angiogenesis. Both MMP-2 and MMP-9 have been detected in not only glioma blood vessels but also glioma cells [18], and their concomitant expression was significantly elevated when the degree of malignancy increased [19]. Peptide sequences such as CGLDD [20], PVGLIG [21] and PLGLAG [22] can also be cleaved by MMP-2 and MMP-9. Based on these background and learned from the ACPP strategy, in the present work, we designed and constructed activatable low molecular weight protamine (ALWMP, E_{10}-PLGLAG-VSRRRRRRGGRRRR) in which the positive charges on the LWMP necessary for transduction were initially masked by a polyanionic peptide ($E10$) via a MMP-2/9-cleavable peptide linker sequence PLGLAG to serve as an ACPP that possess glioma homing ability. Considering the dramatically upregulated expression of MMP-2 and MMP-9 in glioblastomas, we speculated that ALMWP held considerable potential for application in anti-glioblastoma drug delivery.

Paclitaxel (PTX) has demonstrable antitumor activity in glioma cell lines and animal model system of brain tumor [23–25], acting by stabilizing the microtubule cytoskeleton and blocking the transit of cycling cells from the G2-phase to the M-phase [26]. However, its clinical application in anti-glioblastoma is limited due to its poor BBB/BTB permeability and the serious side effects associated with administration of the paclitaxel solvent, Cremophor EL [27].

In this work, using poly(ethylene glycol)-poly(ε-caprolactone) block copolymer (PEG-PCL) as the matrix, a 'smart' DDS was constructed by conjugating ALMWP to the PEG-PCL nanoparticles to strengthen the glioblastoma targeting and tumor penetration of the formulation. The MMP-sensitive targeting effect of PTX-loaded or fluorescently-labeled ALMWP-NP was investigated using both *in vitro* cell and *in vivo* animal model and compared with that of LMWP-NP and unmodified NP.

2. Materials and methods

2.1. Materials

LMWP (CVSRRRRRRGGRRRR) and ALMWP (E_{10}PLGLAGVSRRRRRRGGRRRRC) were synthesized by ChinaPeptides Co., Ltd (Shanghai, China). Methoxy poly(-ethylene glycol) $_{3000}$-poly(ε-caprolactone) $_{20000}$ (MePEG-PCL) and maleimide-poly (ethylene glycol) $_{3400}$-poly(ε-caprolactone) $_{20000}$ (Male-PEG-PCL) were kindly provided by East China University of Science and Technology. Paclitaxel was purchased from Xi'an Sanjiang Bio-Engineering Co. Ltd. (Xi'an, China) and Taxol® from Bristol-Myers Squibb Company. Coumarin-6 and metastat were obtained from Sigma–Aldrich (St. Louis, MO, USA) and 4,6-diamidino-2-phenylindole (DAPI) from Molecular Probes (Eugene, OR, USA). The near-infrared dye, 1, 1′-dioctadecyl-3, 3, 3′, 3′-tetramethyl indotricarbocyanine Iodide (DiR) was provided by Biotium (Hayward, CA). The cell counting kit-8 (CCK-8) was obtained from Dojindo (Kumamoto, Japan).

Dulbecco's modified Eagle's medium (high glucose) (DMEM), fetal bovine serum (FBS), Trypsine-EDTA (0.25%), penicillin-streptomycin and agarose were purchased from Gibco (Invitrogen, USA). Plastic cell culture dishes and plates were obtained from Corning Incorporation (USA). Deionized water (Millipore, Bedford, MA) was used through the entire study. All other reagents were of analytical or chromatographic pure grade and provided by Sinopharm Chemical Reagent Co., Ltd (Shanghai, China).

Rat C6 glioma cell line was purchased from Cell Institute of Chinese Academy of Sciences (Shanghai, China) and maintained in DMEM supplemented with 10% FBS, 100 U/ml penicillin and 100 μg/ml streptomycin at 37 °C in a humidified atmosphere containing 5% CO_2.

Male Spraguee–Dawley (SD) rats (200 ± 20 g) and male BALB/c nude mice (20 ± 2 g) were purchased from the BK Lab Animal Ltd. (Shanghai, China). The animals were maintained under standard housing conditions. All the animal experiments were carried out in accordance with guidelines evaluated and approved by the ethics committee of Fudan University (Shanghai, China).

2.2. Preparation of the nanoparticles

Nanoparticles were prepared with a blend of MePEG-PCL and Maleimide-PEG-PCL using the emulsion/solvent evaporation method as described previously [24]. Briefly, 22.5 mg MePEG-PCL, 2.5 mg Maleimide-PEG-PCL and 0.5 mg PTX were dissolved in 1 ml dichloromethane. Thereafter, 2 ml of an aqueous sodium cholate solution (1%, w/v) was slowly poured into the solution and then the resulting O/W emulsion was formed by sonication (240 w, 50 s) on ice using probe sonicator (Ningbo Scientz Biotechnology Co. Ltd., China). Immediately after sonication, the emulsion was diluted into a 10 ml of sodium cholate solution (0.5%, w/v) under magnetic stirring for 5 min and dichloromethane was rapidly eliminated by evaporation under vacuum. The formed NP was collected by centrifugation at 14500 rpm using a TJ-25 centrifuge (Beckman Counter, USA) at 4 °C for 1 h and washed twice with deionized water in order to completely remove excess sodium cholate. After discarding the supernatant, the NP was resuspended in 1 ml 0.01 M HEPES buffer (pH 7.0) and stored at 4 °C until further use.

The fluorescently-labeled nanoparticles were prepared with the same procedure except that 0.1% of coumarin-6 or 1% of DiR was added to the dichloromethane containing copolymers before primary emulsification. The unentrapped coumarin-6 or DiR was removed via a 1.5 × 20 cm sepharose CL-4B column (Pharmacia Biotech, Inc., Sweden).

Nanoparticles modified with LMWP (LMWP-NP) or ALMWP (ALMWP-NP) were prepared via a maleimide-thiol coupling reaction at room temperature for 8 h as described previously [28]. The products were then eluted with 0.01 M HEPES buffer (pH 7.0) through a 1.5 × 20 cm sepharose CL-4B column to remove the unconjugated peptide.

2.3. Nanoparticles characterization

2.3.1. Particle size distribution and zeta potential

The particle mean size, size distribution and zeta potential of the LMWP-NP and ALMWP-NP were measured with a dynamic light scattering detector (Zetasizer, Nano-ZS, Malvern, UK). The particles size distribution (PSD) was characterized by the intensity averaged particle size and polydispersity index (P.I.).

2.3.2. X-ray photo electron spectroscopy (XPS)

To determine the surface composition of NP, LMWP-NP and ALMWP-NP, the samples were lyophilized using an ALPHA 2-4 Freeze Dryer (0.070 Mbar Vakuum, −80 °C, Martin Christ, Germany) and subjected to XPS analysis. The determination was performed on a RBD upgraded PHI-5000C ESCA system (Perkin Elmer).

2.3.3. Transmission electron microscopy

Morphology of the nanoparticles was characterized via a transmission electron microscope (TEM) (H-600, Hitachi, Japan) following negative staining with 2% sodium phosphotung state solution.

2.3.4. Drug encapsulation efficiency (EE) and loading capacity (LC)

The drug encapsulation efficiency (EE) and loading capacity (LC) of PTX-loaded PEG-PCL nanoparticles (NP-PTX), PTX-loaded PEG-PCL nanoparticles modified with LWMP (LWMP-NP-PTX) and ALWMP (ALWMP-NP-PTX) were investigated as previously described [29].

The EE% and LC% were calculated as indicated below:

$$EE(\%) = \frac{\text{Amount of PTX in the nanoparticles}}{\text{Total amount of PTX added}} \times 100\%$$

$$LC(\%) = \frac{\text{Amount of PTX in nanoparticles}}{\text{nanoparticles weight}} \times 100\%$$

2.3.5. In vitro release profiles

The in vitro release behaviors of PTX from NP-PTX, LWMP-NP-PTX and ALWMP-NP-PTX were evaluated with a dialysis method as described previously [30] using PBS (pH 7.4) with 0.5% Tween-80 as the release medium to create a pseudo-sink condition. For the experiment, 1 ml of the PTX formulation (containing 80 μg PTX) was introduced into a dialysis bag (MWCO 8000 Da, Greenbird Inc., Shanghai, China), the end-sealed dialysis bag was submerged fully into the release medium and incubated at 37 °C at the shaking speed of 120 rpm for 96 h. At appropriate time intervals (0, 1, 2, 3, 4, 6, 8, 12, 24, 48, 72, 96 h), 0.2 ml aliquots were withdrawn and immediately equal amounts of fresh dissolution medium were replenished. Samples were analyzed using the HPLC method as mentioned below.

2.3.6. HPLC analysis

The concentration of PTX in the samples was determined via a Shimadzu LC-10AT HPLC system (Shimadzu, Japan) with a C-18 Diamonsil column (20 mm × 4.6 mm, 5 μm, Dikma, China) [31]. The mobile phase was a mixture of $CH_3OH:H_2O$ (75:25, v/v) at the flow rate of 1.2 ml/min. The sample injection volume was 20 μl and the detection wavelength was 227 nm.

2.4. Cellular uptake in C6 glioma cells

Qualitative evaluation of cellular association of LWMP-NP and ALWMP-NP was observed under a fluorescent microscope, using coumarin-6 as the fluorescent probe. For the experiment, C6 cells were seeded into 24-well plates at the density of 4×10^4 cells per well, incubated for 24 h, and checked under the microscope for confluency and morphology. Cells achieving 70—80% confluence were incubated with coumarin-6-loaded NP, LWMP-NP and ALWMP-NP in serum-free media for 1 h at the concentration of 200 μg/ml at 37 °C. After that, the cells were washed three times with PBS, fixed with 4% formaldehyde for 15 min and visualized under a fluorescent microscope (Leica DMI4000 B, Germany). To determine if the internalization of ALWMP-NP into C6 cells is MMP-2/9 dependent, 1 μM MMP-2/9 inhibitor — metastat was incubated with the cell together with 200 μg/ml ALWMP-NP for 1 h at 37 °C with the cellular associated ALWMP-NP detected and compared with that of non-inhibited control.

Quantitative analysis of cellular association of coumarin-6-loaded NP, LWMP-NP and ALWMP-NP was determined with a High Content Cell Analysis System (HCS). Briefly, C6 cells were seeded in a 96-well plate at the density of 5000 cells/well, cultured for 24 h, and then incubated with coumarin-6-labeled NP, LWMP-NP, ALWMP-NP, a mixture of 1 μM MMP-2/9 inhibitor metastat and LWMP-NP and a mixture of 1 μM MMP-2/9 inhibitor metastat and ALWMP-NP, respectively, for 1 h at 37 °C. After that, the cells were washed with PBS and fixed with 4% formaldehyde solution for 15 min and stained with 2 μg/ml Hochest 33258 at room temperature for 10 min away from light. The cells was finally washed with PBS for three times and detected under a KineticScan® HCS Reader (version 3.1, Cellomics Inc., Pittsburgh, PA, USA).

2.5. Mechanism of cellular uptake of ALMWP-NP

C6 cells were seeded in a 96-well plate at the density of 5000 cells/well and cultured for 24 h. Endocytic inhibitors including 10 μg/ml chlorpromazine, 4 μg/ml colchicines, 10 μg/ml cyto-D, 5 μg/ml BFA, 5 μg/ml filipin, 10 mM NaN₃, 50 mM deoxyglucose, 2.5 mM methyl-β-cyclodextrin (M-β-CD), 200 nM monensin, and 20 μM nocodazole were incubated with the cells for 30 min, respectively, before their incubation with ALMWP-NP (200 μg/ml, 1 h, 37 °C). Quantitative analysis of the cellular association of nanoparticles following the inhibitor treatments was performed as abovementioned and compared with that of the non-inhibited control.

2.6. Tumor spheroid penetration

In order to further evaluate the tumor penetrating ability of ALMWP-NP, three-dimensional spheroids of C6 glioma cells were cultured as described previously [32]. Agarose solution was prepared in serum-free DMEM (2%, w/v) by heating at 80 °C for 30 min. C6 cells were seeded at a density of 2×10^3 cells/400 μl per well in the 48-well plates coated with 150 μl of 2% agarose solution. Subsequently, plates were gently agitated for 5 min on the first day. Seven days after the cells were seeded, the formed tumor spheroids were incubated with 500 μg/ml coumarin-6-loaded NP,

LMWP-NP or ALMWP-NP, respectively. Four hours later, the spheroids were rinsed three times with ice-cold PBS and fixed with 4% paraformaldehyde for 30 min. Then, the spheroids were transferred to glass slides with the nanoparticle penetration observed under a laser scanning confocal microscope (Zeiss LSM 510).

2.7. Anti-proliferation assay

C6 cells were seeded into 96-well plates at the density of 5000 cells/well and incubated for 24 h at 37 °C in a 5% CO_2 atmosphere to allow cell attachment. After that, the medium was refreshed with 200 μl serum-free medium containing Taxol®, NP-PTX, LWMP-NP-PTX and ALWMP-NP-PTX, respectively, at the PTX concentrations ranging from 1 ng to 10 μg. Cells without exposure to the PTX formulations were used as control. After 72 h incubation, cell viability was evaluated via Cell Counting Kit-8 (CCK-8) assay according to the manufacturer's instruction.

2.8. Pharmacokinetic studies

Sixteen male SD rats weighting 200 ± 20 g were randomly divided into four groups and intravenously administrated via the tail vein with Taxol®, NP-PTX, LWMP-NP-PTX, ALWMP-NP-PTX respectively at an equivalent dose of 5 mg/kg PTX. Blood samples were drawn from the carotid vein at 0.083, 0.25, 0.5, 1, 2, 3, 4, 6, 8, 12 and 24 h post-injection. The plasma samples were collected following centrifugation at 3000 rpm for 10 min and stored at −20 °C until assays.

To prepare samples for analysis, 200 μl methanol containing 60 ng/ml docetaxel (internal standard) was added into 50 μl plasma to precipitate the proteins. The mixture was vortexed and subsequently centrifuged at 12000 rpm for 10 min with the supernatant mixed with an equal volume of deionized water and subjected to liquid chromatography-tandem mass spectrometry (LC−MS/MS) analysis as described previously [33]. Detection of the ions was conducted in the multiple reaction monitoring (MRM) mode, monitoring the transition of the m/z 876.6 → 308.0 for paclitaxel $(M + Na)^+$ and 830.3 → 549.1 for docetaxel $(M + Na)^+$, respectively. All the concentration data were dose-normalized and plotted as plasma drug concentration−time curves. The pharmacokinetic data analysis was performed by means of a model independent method [34].

2.9. Tissue biodistribution

Tissue biodistribution and tumor targeting properties of ALWMP-NP-PTX was performed on nude mice bearing glioma xenograft, and compared with that of LMWP-NP-PTX, NP-PTX and Taxol®. The C6 glioma model was established by inoculation of 1×10^7 cells (in 200 μl cell culture medium) into the subcutaneous tissue of the armpit of right anterior limb. When the size of tumors reached 0.4−0.6 cm in diameter, the mice were considered ready for treatment and randomly divided into four groups, intravenously administrated with Taxol®, NP-PTX, LWMP-NP-PTX, ALWMP-NP-PTX at a dose of 5 mg/kg PTX, respectively. At predestinate time points (0.5, 1, 3, 6, 12 and 24 h) post-injection, three mice of each group were sacrificed with the heart, liver, spleen, lung, kidney, brain, and tumor collected and stored at −20 °C until analysis.

For drug concentration detection, the organ samples were homogenized in 3-fold volumes of distilled water with the homogenate pretreated via protein precipitation procedure using docetaxel as the internal standard and the supernatant following centrifugation subjected to LC-MS/MS analysis as described above.

2.10. In vivo imaging

Near-infrared dye DiR was applied as the fluorescence probe for evaluating the targeting efficiency of to the intracranial C6 orthotopic glioma allograft. C6 cells (5.0×10^5 cells suspended in 5 μl PBS) were implanted into the right striatum (1.8 mm lateral to the bregma at 3 mm depth) of male BALB/c nude mice using a stereotactic fixation device equipped with a mouse adapter. The intracranial C6 glioma-bearing mice were injected with 200 μl DiR-loaded NP, LWMP-NP or ALWMP-NP (1 mg/kg) via the tail vein fourteen days after implantation. The fluorescent images were detected using a CRi in vivo imaging system (CRi, MA, USA) at predetermined time points. Twenty-four hours after administration, the mice were sacrificed with the hearts, livers, spleens, lungs, kidneys and tumor-bearing brains dissected, washed with saline, and visualized under the CRi in vitro imaging system.

2.11. In vivo glioma distribution

BALB/c mice bearing intracranial C6 glioma were established as described above. Fourteen days after implantation, coumarin-6-loaded NP, LWMP-NP or ALWMP-NP was injected into the tail vein of mice at an equal dose of coumarin-6. At 3 h post-injection, the mice were anesthetized with i.p. administered 5% chloral hydrate, fixed by heart perfusion with saline and 4% paraformaldehyde. Then the brains were removed, fixed in 4% paraformaldehyde for 48 h, dehydrated with 15% sucrose solution for 24 h and 30% sucrose solution for 24 h sequentially until subsidence. Afterward, the brains were embedded in OCT (Sakura, Torrance, CA, USA) and frozen at −80 °C, sectioned at 20 μm. Following counterstaining with DAPI (100 ng/ml) for 10 min and triple rinsing with PBS, slides were visualized under a Zeiss LSM 510 confocal microscope.

2.12. Anti-glioma activity

Mice bearing intracranial C6 glioma were established as described in section 2.10. The mice were randomly divided into five groups, treated with ALWMP-NP-PTX, LWMP-NP-PTX, NP-PTX and Taxol® (at a dose of 5 mg/kg PTX) and physiological saline, respectively, at 7, 10, 13, 16, 19 and 22 days after implantation with the survival times recorded [26].

2.13. Statistical analysis

All the data were presented as mean ± SD and comparison among the different groups was performed by one-way ANOVA followed by Bonferroni tests. The IC_{50} values were calculated by nonlinear regression analysis with the GraphPad Prism® 5.0 version program. The probability of survival was estimated by the Kaplan–Meier method and compared by the log-rank test. Statistical significance was defined as $p < 0.05$.

3. Results

3.1. Characterization of the nanoparticles

The mean diameters of NP-PTX, LMWP-NP-PTX and ALMWP-NP-PTX were around 107 nm, 134 nm, 121 nm, respectively, with acceptable polydispersity index (P.I. = 0.091, P.I. = 0.185, P.I. = 0.136, respectively) (Fig. 1A,B,C). The conjugation with LWMP or ALWMP slightly increased the particle sizes. Particles exhibited spherical shape of moderate uniform particle size as observed under TEM (Fig. 1D,E,F).

The zeta potentials were −23.3 ± 0.82 mV, +18.4 ± 1.75 mV and −21.8 ± 1.28 mV for NP-PTX, LMWP-NP-PTX, ALMWP-NP-PTX, respectively. The existence of LMWP on the surface of LMWP-NP and ALMWP on the surface of ALMWP-NP was confirmed by XPS analysis which showed 1.35% nitrogen on the LMWP-NP surface and 1.83% nitrogen on the ALMWP-NP surface while that on the surface of unconjugated NP undetectable.

The LC of NP, LMWP-NP and ALMWP-NP was 1.29 ± 0.05%, 1.23 ± 0.08% and 1.20 ± 0.05%, respectively. And the EE of PTX was 49.8 ± 3.4%, 48.7 ± 3.8% and 47.5 ± 3.9% for NP, LMWP-NP and ALMWP-NP, respectively.

The *in vitro* release profiles of NP-PTX, LMWP-NP-PTX and ALMWP-NP-PTX displayed a similar biphasic pattern (Fig. 1G), which was characterized by a fast initial release within the first 24 h (about 50% release) and a slower and continuous release in the following 72 h (75% total release).

3.2. Cellular uptake in C6 glioma cells

Qualitative fluorescent microscopy analysis showed that the cellular associated fluorescence intensity for LMWP-NP and
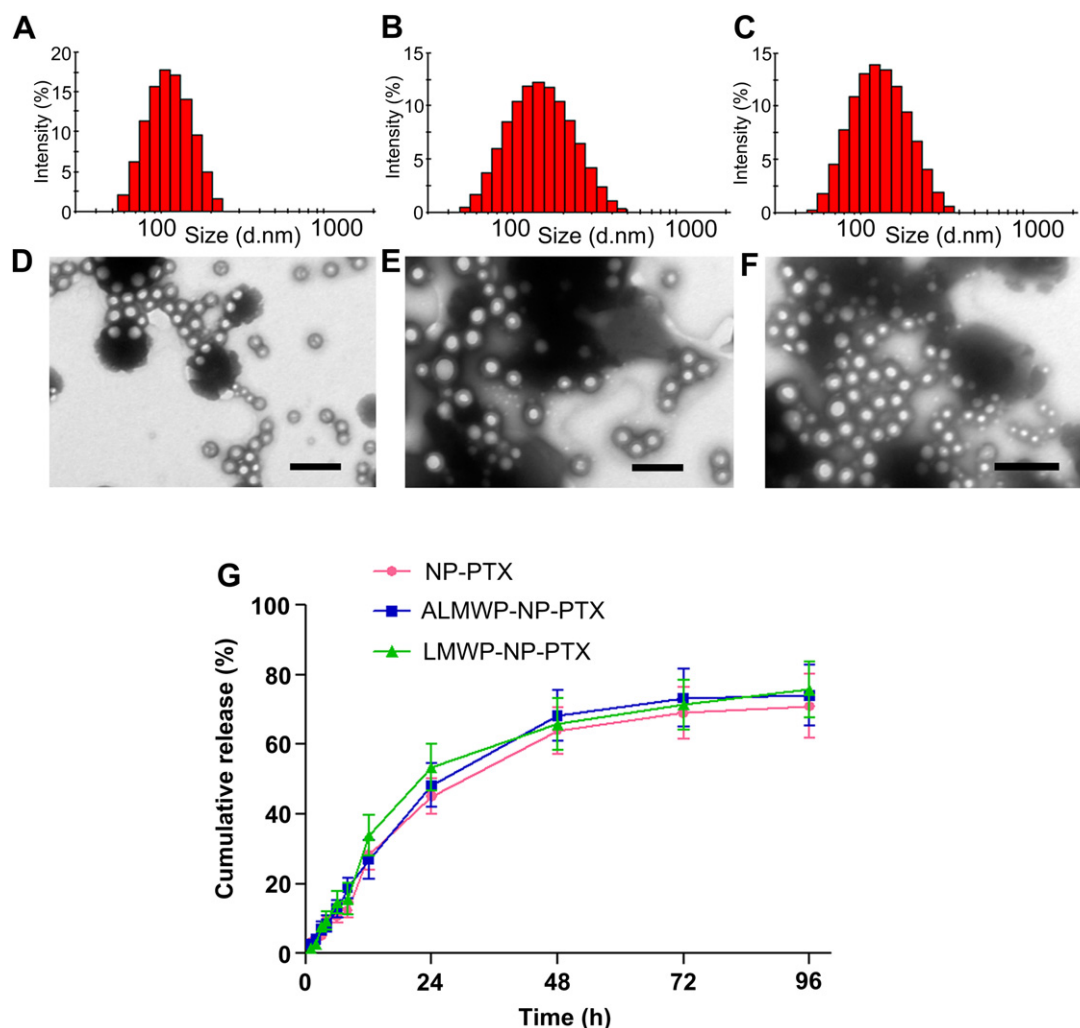

Fig. 1. Characterization of NP, LMWP-NP and ALMWP-NP. Particle size distribution and TEM image of NP (A, D), LMWP-NP (B, D) and ALMWP-NP (C, F). PTX release profiles from NP-PTX, LMWP-NP-PTX and ALMWP-NP-PTX in PBS (pH 7.4) with 0.5% Tween-80 at 37 °C (G). The bar is 200 nm.

ALMWP-NP was significantly higher than that of NP. The cellular accumulation of ALMWP-NP was as high as that of LMWP-NP. Furthermore, the cellular uptake of ALMWP-NP was significantly inhibited by MMP inhibitor. (Fig. 2).

These results were confirmed by the quantitative HCS analysis. The uptake of LMWP-NP and ALMWP-NP was 3.75 and 3.39 folds, respectively, when compared with that of the unmodified NPs. The presence of MMP-2/9 inhibitor metastat significantly reduced cellular association of ALMWP-NP ($p < 0.001$), but showed no effect on the cellular uptake of LMWP-NP. Although ALMWP-NP internalization was slightly lower than that of LMWP-NP, no significant difference between them was detected (Fig. 3).

3.3. C6 cellular uptake mechanism of ALMWP-NP

As shown in Fig. 4, microtubules depolymerization agent — colchicines and nocodazole significantly reduced the cellular uptake of ALMWP-NP in C6 cells ($p < 0.05$, $p < 0.001$, respectively), while caveolae-mediated endocytosis pathway inhibitor — filipin and clathrin-mediated endocytosis pathway inhibitor — chlorpromazine did not influenced the cellular uptake of ALMWP-NP evidently ($P > 0.05$). Energy-depletion agent — NaN$_3$ and lipid raft inhibitor — M-β-CD was observed to decrease the internalization of ALMWP-NP by 60.4% and 74.6% ($p < 0.001$), respectively. Furthermore, Golgi apparatus destroyer — BFA and lysosome
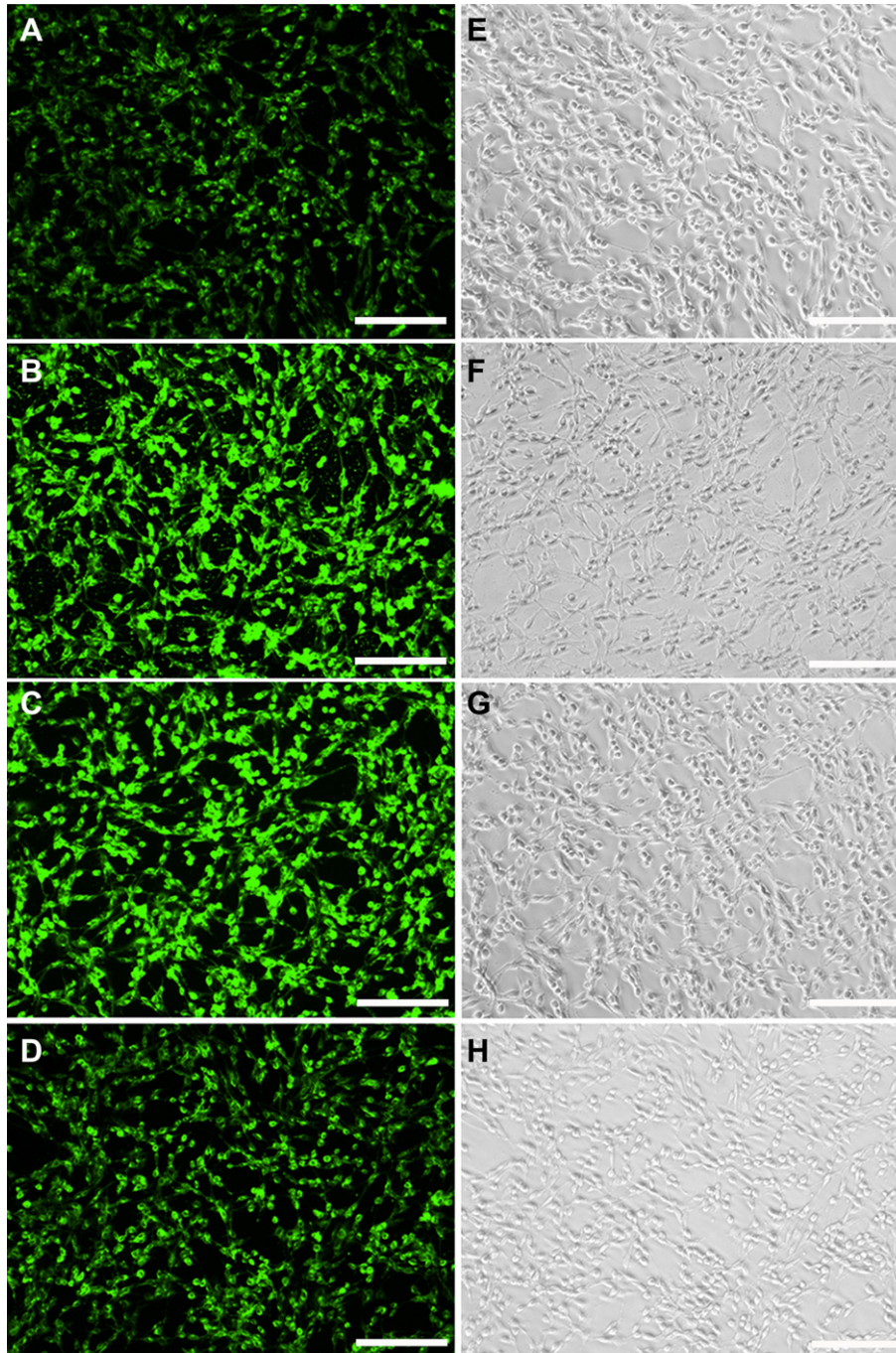
Fig. 2. Cellular associated fluorescent signal from the nanoparticles after a 1 h incubation with 200 μg/ml coumarin-6-labeled NP (A, E), LMWP-NP (B, F), ALMWP-NP (C, G) and ALMWP-NP in the presence of 1 μM MMP inhibitor metastat (D, H). The bar is 100 μm.
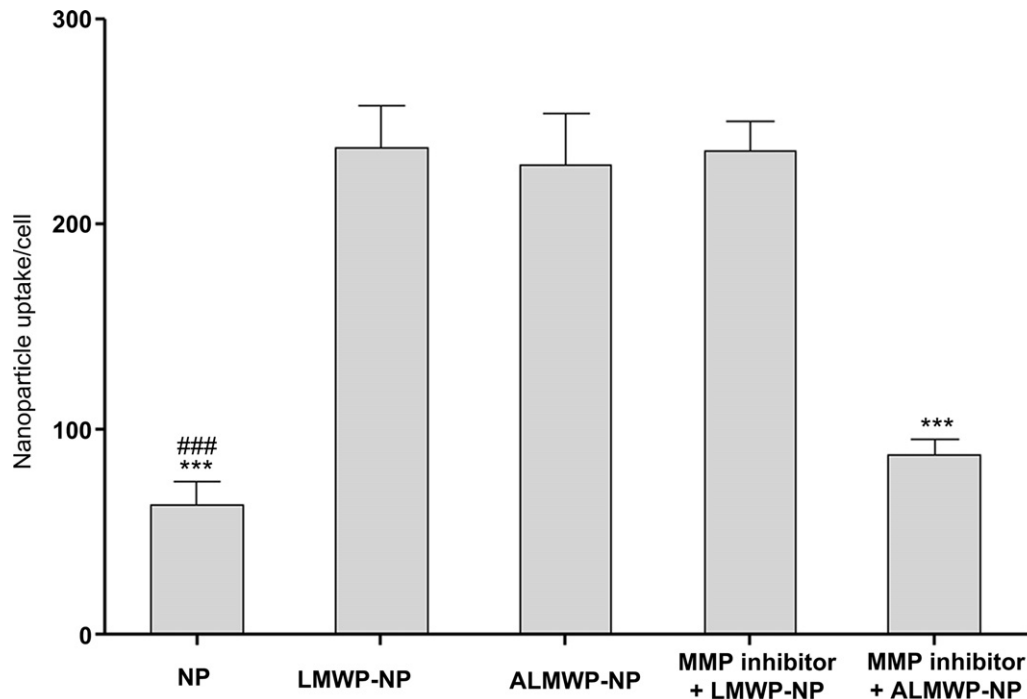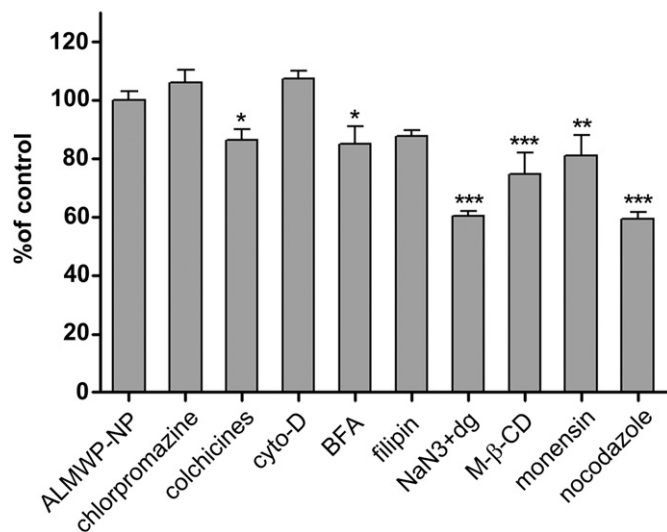
Fig. 3. Quantitative analysis of the cellular associated nanoparticles following a 1 h incubation with 200 μg/ml coumarin-6-labeled NP, LMWP-NP in the absence/presence of 1 μM MMP inhibitor metastat, ALMWP-NP in the absence/presence of 1 μM MMP inhibitor metastat. Values expressed as mean ± SD. ***$p < 0.001$, significantly lower than the cellular association of coumarin-6-loaded ALMWP-NP. ###$p < 0.001$, significantly lower than the cellular association of coumarin-6-loaded LMWP-NP.

inhibitor − monensin also significantly suppressed the transcytosis of ALMWP-NP ($p < 0.05$, $p < 0.01$, respectively).

3.4. Tumor spheroid penetration

As targeting DDS is optimal to be transported deeper into glioma regions, in addition to the cellular uptake experiments, penetration in C6 glioma spheroid was also evaluated to determine

Fig. 4. Cellular uptake of coumarin-6-labeled ALMWP-NP in C6 glioma cells in the presence of chlorpromazine (10 μg/ml), colchicines (4 μg/ml), cyto-D (10 μg/ml), BFA (5 μg/ml), filipin (5 μg/ml), NaN₃ (10 mM) together with deoxyglucose (50 mM), M-β-CD (2.5 mM), monensin (200 nM) and nocodazole (20 μM), respectively. Fluorescence intensity of coumarin-6 in the non-inhibited cells, representing the maximum internalized amount of coumarin-6-labeled ALMWP-NP, was taken as control. *$p < 0.05$, **$p < 0.01$, ***$p < 0.001$ significantly different with the non-inhibited control ($n = 3$).

the penetrating efficacy of ALMWP-NP. As showed by confocal microscopy analysis, NP, LMWP-NP and ALMWP-NP penetrated into C6 spheroids with 105.15 μm, 133.36 μm and 130.87 μm in depth, respectively (Fig. 5A,C,E). LMWP-NP and ALMWP-NP penetrated deeper and distributed more extensive in the spheroids than NP, suggesting that LMWP and ALMWP modification could effectively increase tumor penetration of nanoparticles (Fig. 5B,D,F).

3.5. Anti-proliferation assay

The anti-proliferative effect of different PTX formulations on C6 cells was evaluated by CCK-8 assay. A strong growth inhibition of C6 cells was found in all the PTX formulations, with IC$_{50}$ values for Taxol®, NP-PTX, LWMP-NP-PTX and ALWMP-NP-PTX being 154.88 nM, 120.23 nM, 35.64 nM and 39.17 nM, respectively (Fig. 6). The IC$_{50}$ value of LMWP-NP-PTX and ALMWP-NP-PTX was similar and 3.37 and 3.07 folds lower than that of NP-PTX, respectively.

3.6. Pharmacokinetic studies

The mean plasma concentration-time profiles of the formulations after intravenous administration to SD rats were illustrated in Fig. 7. It was found that NP-PTX and ALMWP-NP-PTX showed similar blood concentration−time curves. Both NP-PTX and ALMWP-NP-PTX showed initial high blood circulating levels, while PTX formulated in Taxol® and LMWP-NP-PTX was quickly cleared from the systemic circulation. The pharmacokinetic data analysis was performed by means of a model independent method and the corresponding pharmacokinetic parameters (AUC(0−t), t$_{1/2}$, k, CL) were presented in Table 1. ALMWP-NP-PTX demonstrated significantly slower clearance rate (CL) ($p < 0.001$) and higher AUC (4.7 folds, $p < 0.001$) when compared with LMWP-NP-
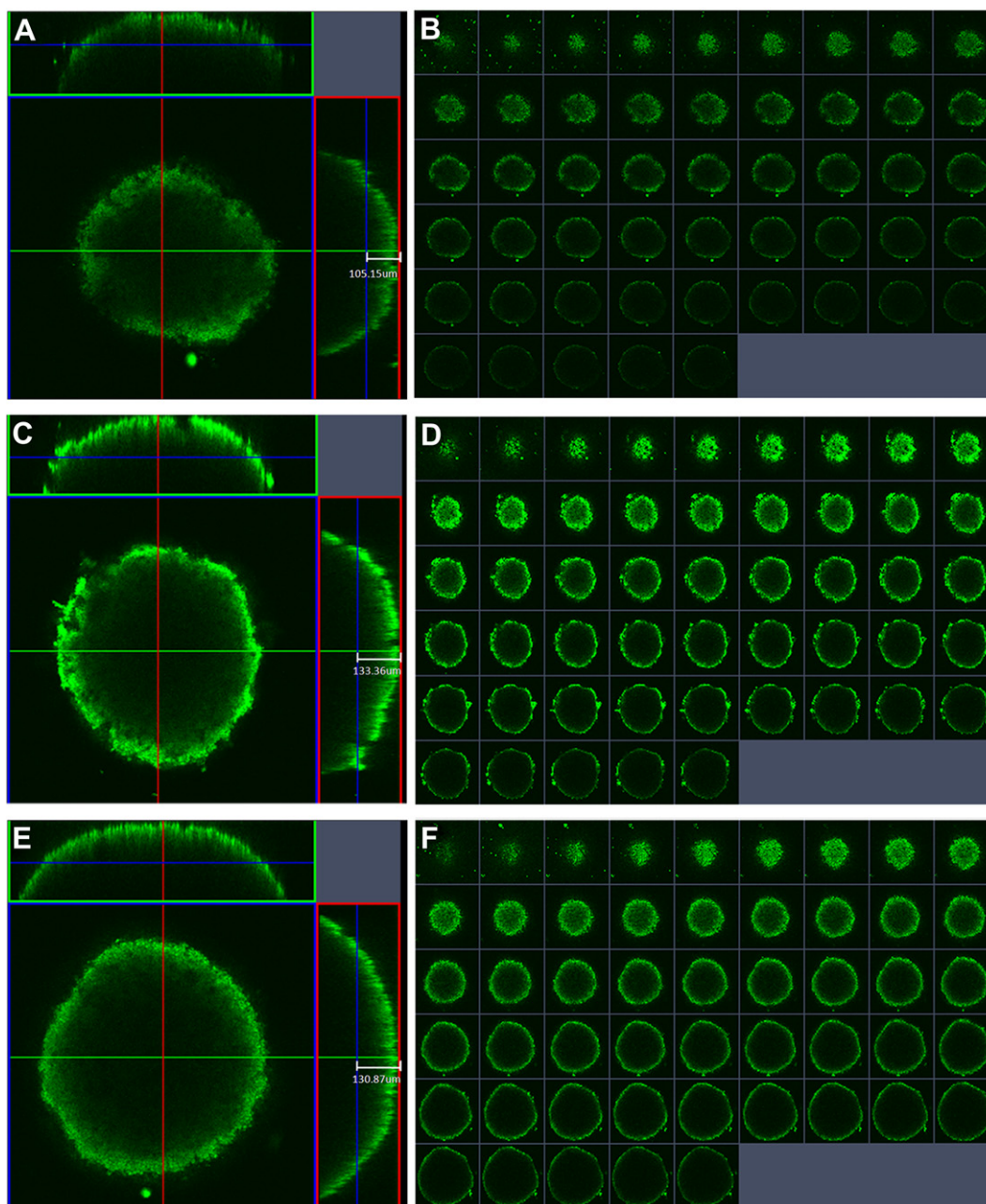
Fig. 5. Nanoparticles penetration in C6 glioma spheroids. The C6 glioma spheroids were incubated with 500 μg/ml coumarin-6-loaded NP (A, B), LMWP-NP (C, D) and ALMWP-NP (E, F), respectively for 4 h. A, C, E, penetration in the X, Y and Z direction; B, D, F, slides from top to bottom.

PTX. Furthermore, no significant difference in CL and AUC was observed between NP-PTX and ALMWP-NP-PTX.

3.7. Biodistribution

Tissue distribution was assessed in mice subcutaneously implanted with C6 glioma tumors following intravenous administration of Taxol®, NP-PTX, LMWP-NP-PTX and ALMWP-NP-PTX, respectively. As shown in Fig. 8, the concentrations of PTX in the tumor of ALMWP-NP-PTX at 0.5, 1, 3, 6, 12, 24 h were 2.31, 3.73, 2.90, 2.20, 2.77, 2.86-fold over that of Taxol®, 2.02, 2.49, 2.40, 1.79, 2.49, 2.74-fold over that of NP-PTX, and 1.65, 1.90, 2.18, 2.28, 3.07, 3.21-fold over that of LMWP-NP-PTX, respectively. Furthermore, ALMWP-NP exhibited a similar biodistribution profile with the unmodified NP in the non-targeted tissues, while a significantly higher level of LMWP-NP was observed accumulate in the liver, heart, spleen and lung.

3.8. In vivo imaging

The glioma-targeting efficiency of NP, LMWP-NP and ALMWP-NP was also investigated in intracranial C6 glioma-bearing nude mice. After the DiR-labeled nanoparticles were given through the tail vein, time-dependent biodistribution of the different nanoparticles were observed using non-invasive NIR fluorescence imaging in live animals. The fluorescent signals detected in the intracranial tumor followed the order of ALMWP-NP > LMWP-NP > NP (Fig. 9). The fluorescence intensity of ALMWP-NP in intracranial tumor site was much stronger than that of NP and LMWP-NP at all the time points from 2 h to 24 h following administration.
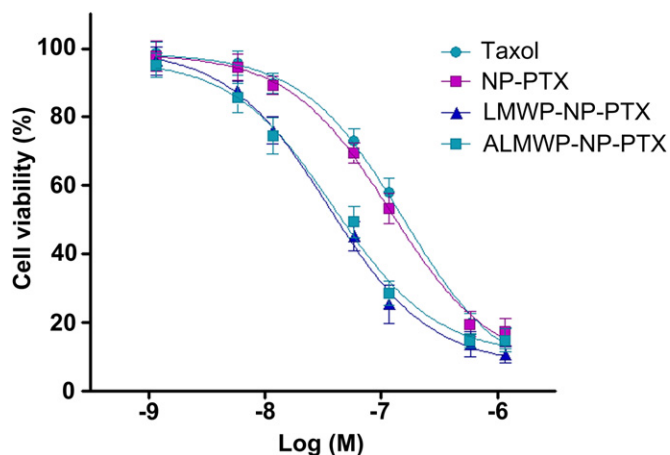
Fig. 6. *In vitro* cytotoxic of various paclitaxel formulations on C6 glioma cells. The C6 cells were plated at 5000 cells per well in the 96-well plate and cultured in growth medium for 24 h prior to exposure to Taxol®, NP-PTX, LWMP-NP-PTX and ALWMP-NP-PTX for 72 h at 37 °C.
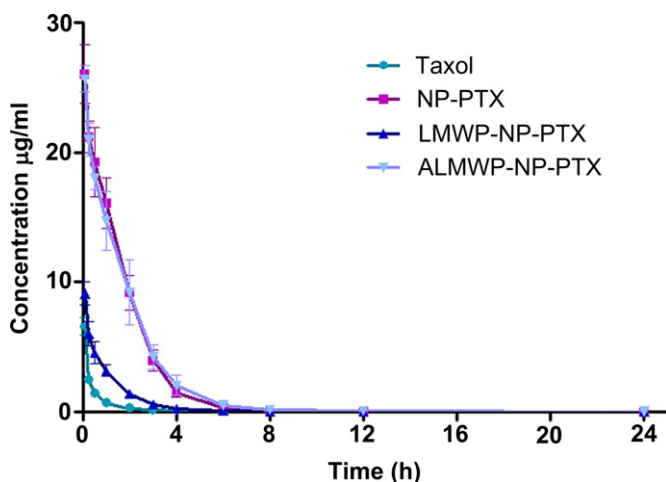
Fig. 7. PTX concentration-time profile following intravenous administration of Taxol®, NP-PTX, LMWP-NP-PTX and ALMWP-NP-PTX in SD rats at the PTX dose of 5 mg/kg, respectively (n = 4).

3.9. In vivo glioma distribution

As shown in Fig. 10, only a low accumulation of NP was observed in the glioma and no obviously distribution in the normal brain tissue (Fig. 10A–C). LMWP-NP showed a slightly higher accumulation in the glioma but also non-selective distribution in the normal brain (Fig. 10D–F). In contrast, the highest amount of ALMWP-NP was observed homed to glioma at dramatically higher level than that in normal brain tissue (Fig. 10G–I).

3.10. Anti-glioma activity

The anti-glioma effect was reflected by the median survival time in the mice bearing intracranial C6 glioma. As shown in Fig. 11, the median survival time of physiological saline group, Taxol® group, NP-PTX group, LMWP-NP-PTX group and the ALMWP-NP-PTX one were 20.5, 24, 30, 34.5 and 48 days, respectively. ALMWP-NP-PTX significantly prolonged animal survival when compare with saline ($p < 0.01$ log-rank analysis), Taxol® ($p < 0.01$), NP-PTX ($p < 0.01$) and LMWP-NP-PTX ($p < 0.05$). When compare with Taxol®, LMWP-NP-PTX ($p < 0.05$) and NP-PTX ($p < 0.05$) also displayed significant prolongation in the survival time. However, no significant difference was observed between the LMWP-NP-PTX group and the NP-PTX one ($p > 0.05$).

4. Discussion

The 5-year survival rate for glioblastoma has been a dismal 4% for the past few decades. Significant breakthroughs in treatment of glioblastoma are still lacking and will come from more rational targeting strategies [35]. Increasing attention has been paid to the potential of CPPs for the efficiently delivery of nanoparticles into brain or glioma tissues [36–38]. As one of the CPPs, LMWP has received increasing interest due to its excellent advantages aforementioned.

In our study, we constructed a MMP sensitive ALMWP by masking positive charges on the LMWP through a polyanionic peptide (E10), linked by MMP2/9-cleavable sequence PLGLAG. ALMWP was conjugated to PEG-PCL nanoparticles via a maleimide-mediated covalent binding procedure, and applied for anti-glioblastoma therapy via i.v. administration. The MMP-2/9 present in glioblastomas act as a scissor to cut the linker, releasing the polycationic LMWP portion and associated nanoparticle to adhere to and be taken up into cells in the immediate vicinity of the protease. PCL was chosen as drug carrier as it is a biodegradable polymer approved for human use by U.S. FDA and widely used in drug delivery applications [39].

The nanoparticles prepared from blends of MePEG-PCL and maleimide-PEG-PCL exhibited an average diameter of around 107 nm, which increased to around 121 nm, 134 nm after ALMWP and LMWP conjugation, respectively. The sizes were all below 150 nm that were regarded as favorable to brain transport [40]. The existence of LMWP on the surface of LMWP-NP and ALMWP on the surface of ALMWP-NP was also verified by an XPS analysis which showed 1.35%, 1.83% nitrogen on the nanoparticle surface of LMWP-NP and ALMWP-NP, respectively. The *in vitro* release results suggest that the moderate modification of LMWP or ALMWP did not evidently influence the *in vitro* release behavior of PEG-PCL nanoparticles.

The zeta potentials of NP-PTX, LMWP-NP-PTX and ALMWP-NP-PTX were -23.3 ± 0.82 mV, $+18.4 \pm 1.75$ mV and -21.8 ± 1.28 mV, respectively, suggesting that the conjugated peptide LMWP contributed to a notable change in zeta potential. The positively charged LMWP-NP could result in a rapid blood clearance and

Table 1
Pharmacokinetic parameters of PTX following intravenous administration of Taxol®, NP-PTX, LMWP-NP-PTX and ALMWP-NP-PTX in SD rats at the PTX dose of 5 mg/kg (n = 4).

Parameters	Taxol®	NP-PTX	LMWP-NP-PTX	ALMWP-NP-PTX
$AUC_{(0-t)}$(mg/L/h)	3.378 ± 0.141***	44.090 ± 0.392	9.413 ± 1.534***	44.229 ± 6.527
$t_{1/2}$ (h)	2.894 ± 0.848**	7.190 ± 0.428	5.653 ± 0.752	6.121 ± 0.436
k(h^{-1})	0.254 ± 0.077*	0.096 ± 0.006	0.113 ± 0.008	0.124 ± 0.017
CL (L/h/kg)	1.482 ± 0.062***	0.114 ± 0.010	0.541 ± 0.088***	0.115 ± 0.016***

*$p < 0.05$, **$p < 0.01$, ***$p < 0.001$ significant different with that of ALMWP-NP-PTX.

a high accumulation in the lung and liver [41], which was confirmed by our pharmacokinetic studies and tissue biodistribution experiments. Pharmacokinetic results indicated that the LMWP-NP-PTX was quickly cleared from the systemic circulation while ALMWP-NP-PTX and NP-PTX exhibited a markedly delayed blood clearance (Fig. 7). The CL for LMWP-NP-PTX was significantly higher than that of ALMWP-NP-PTX ($p < 0.001$) (Table 1). Meanwhile, ALMWP-NP-PTX and NP-PTX showed similar
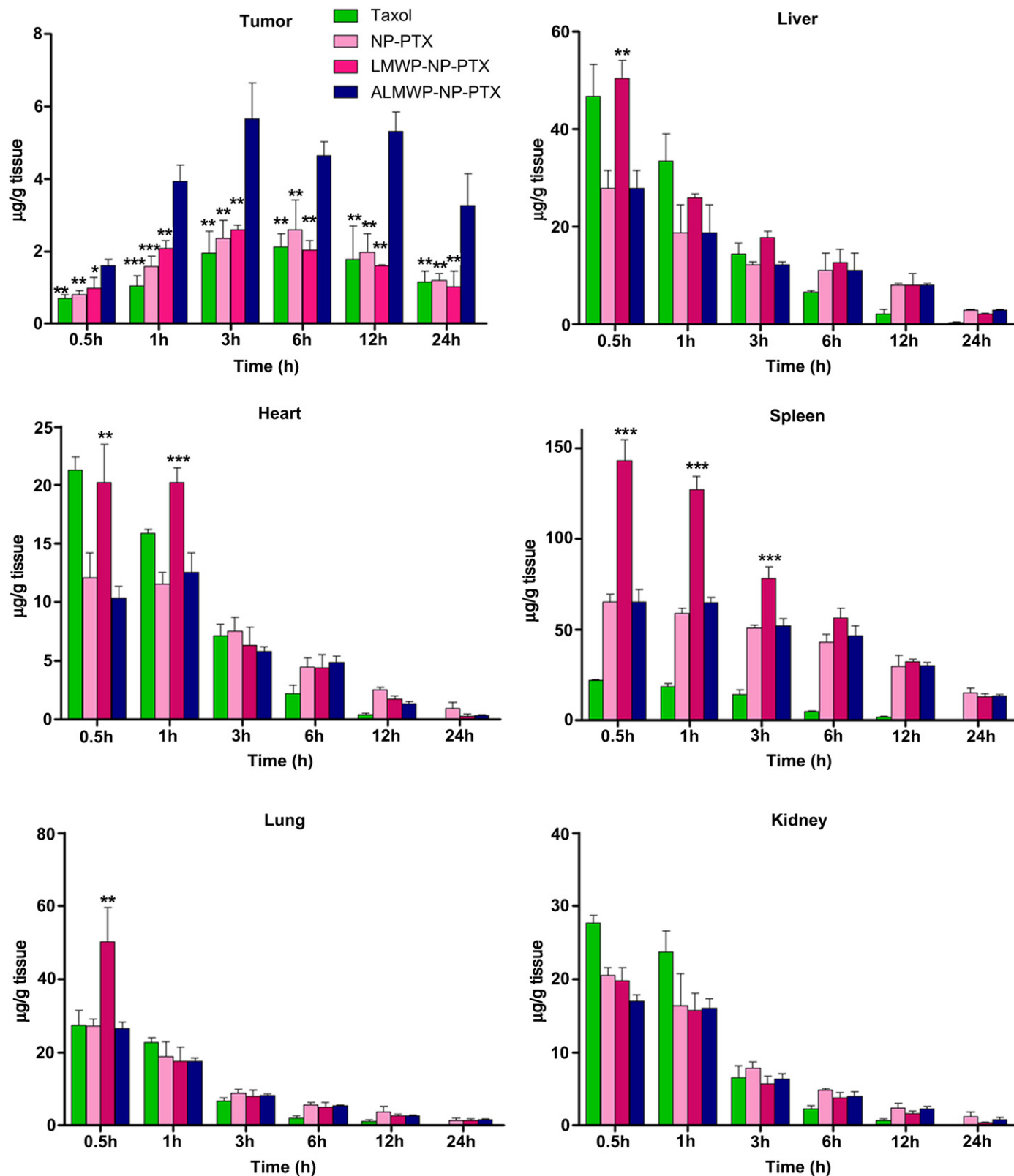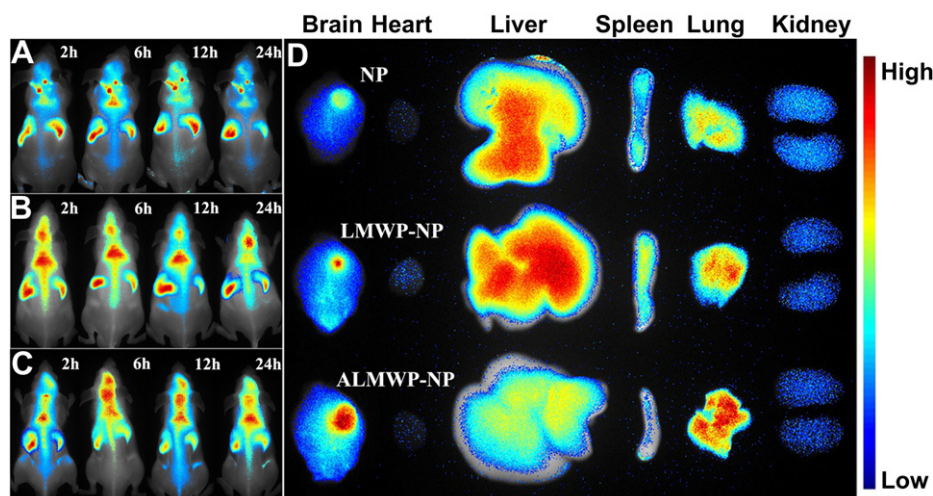

Fig. 8. Tissue biodistribution of Taxol®, NP-PTX, LMWP-NP-PTX and ALMWP-NP-PTX in mice bearing C6 glioma xenograft at 0.5, 1, 3, 6, 12, and 24 h after intravenous injection ($n = 3$ for each group at each time point). *$P < 0.05$, **$P < 0.01$, ***$p < 0.001$ significantly different with that of ALMWP-NP-PTX. All error bars reflect SD.

Fig. 9. *In vivo* fluorescence imaging of intracranial C6 glioma-bearing nude mice after intravenous injection with DiR-labeled NP (A), LMWP-NP (B) and ALMWP-NP (C). Images of dissected organs of mice bearing intracranial C6 glioma sacrificed 24 h after intravenous injection of nanoparticles (D).

blood concentration—time curves, suggesting the conjugation of an adequate amount of ALMWP on the surface of NP did not impair the long-circulation characteristic of PEG. Biodistribution study in xenograft nude mouse models showed that high accumulation of LMWP-NP-PTX was found in non-targeted tissues, including liver, heart, lung and spleen (Fig. 8). On the contrary, ALMWP-NP exhibited a similar biodistribution profile with unmodified NP, as the absence of cell specificity of LMWP was shielded by polyanion. Taken together, ALMWP-NP-PTX possesses a desirable pharmaco-kinetic and biodistribution profiles, making it suitable for *in vivo* glioma targeting drug delivery via systemic administration.

In vitro cell experiments were performed on C6 glioma cells as C6 glioma is very close to human multiform glioblastoma by morphology, characteristics of invasive growth and spectrum of expressed proteins [42]. In the meanwhile, MMP-2 and MMP-9 has been noted to over-expressed in rat C6 glioma cells [43,44], and also in human glioblastomas as compared to low-grade gliomas and normal brains [45]. As shown in Figs. 2 and 3, cellular uptake of PEG-PCL nanoparticles in C6 cells was significantly enhanced following surface conjugation with both LMWP and ALMWP. Furthermore, MMP inhibitor significantly suppressed the cellular uptake of ALMWP-NP, but exerted no effect on LMWP-NP, con-firming that the enhanced cellular internalization of ALMWP-NP is activated by the tumor-specifically over-expressed extracellular MMP-2/9. In addition, the cellular association of ALMWP-NP was almost at the same level with that of LMWP-NP, which is in consistent with previous reports that claimed proteases are cata-lytic enzymes, and one protease molecule can specifically activate hundreds, or even thousands of its substrates [46].

Understanding the cellular entry of nanomedicines has become central to the field of drug delivery. Endocytic inhibitors including clathrin-mediated endocytosis pathway inhibitor — chlorproma-zine, caveolae-mediated endocytosis pathway inhibitor — filipin, Golgi apparatus destroyer — BFA, lysosome inhibitor — monensin, lipid raft inhibitor — M-β-CD, microtubules depolymerization agent — colchicines and nocodazole, and energy-depletion agent — NaN$_3$ were explored to characterize the endocytosis pathways involved in the C6 cellular uptake of ALMWP-NP [28,47,48]. It was found that colchicines, nocodazole and NaN$_3$ significantly reduced the cellular uptake of ALMWP-NP (Fig. 4), indicating that energy-dependent macropinocytosis played an important role in the cellular uptake of ALMWP-NP. The cellular association of ALMWP-NP was also inhibited by M-β-CD, suggesting that lipid raft-

mediated endocytosis also involved in the cellular transport. In addition, BFA and monensin reduced the internalization of ALMWP-NP, confirming the involvement of both Golgi apparatus and lysosome in the intracellular transport of ALMWP-NP. Taken together, our findings supported that ALMWP-NP internalization within C6 cells was mediated by more than one cellular uptake mechanisms, involving lipid raft-mediated endocytosis and energy-dependent macropinocytosis. The use of specific ligands such as RGD [30], Angiopep [49] and WGA [47] that usually mediated the transport associated nanoparticles into targeted cells via clathrin-mediated endocytosis could eventually lead to a complete degra-dation of nanoparticles at the later lysosomal stage [50]. In contrast, the fact that the majority of ALMWP-NP is taken up by C6 cells via the nondestructive routes is indeed encouraging.

The active protease-dependent glioma targeting effects of ALMWP-NP was further confirmed by *in vivo* imaging experiment in which nude mice bearing intracranial C6 glioma were used as the animal model. Accumulation of ALMWP-NP in intracranial tumor site was much higher than that of NP and LMWP-NP at all the time points, suggesting that active protease-dependent accumulation make a significant contribution beyond EPR effect (Fig. 9). These results were in good consistent with qualitative biodistribution study which showed that at all time points, animals received the ALMWP-NP-PTX showed the highest PTX accumulation at the tumor site. These data together strongly confirmed the protease-sensitive glioma targeting ability of ALMWP.

In vivo glioma distribution of the functinalized nanoparticles were examined under confocal microscopy. It was demonstrated that a low accumulation of unmodified NP was observed in the central tumor site, which could be contributed by the leaky vascular wall at the core of glioma. LMWP-NP showed a slightly higher accumulation in the glioma but also non-selective distri-bution in the normal brain, indicating that the cationic charged LWMP facilitate the interaction between the nanoparticles and both the normally charged BBB and tumor vessels. In contrast, ALMWP-NP showed the highest distribution selectively in the glioma regions (Fig. 10), which is believed to be contributed by the higher express of MMP-2/9 in the tumor neovasculature as well as the glioma cells than that in normal brain tissues. These results demonstrated that LMWP could enable transvascular delivery of nanoparticles to both normal brain tissue and glioma without significantly selectivity, while ALMWP provided a notable glioma-targeted delivery of nanoparticles with high efficacy.
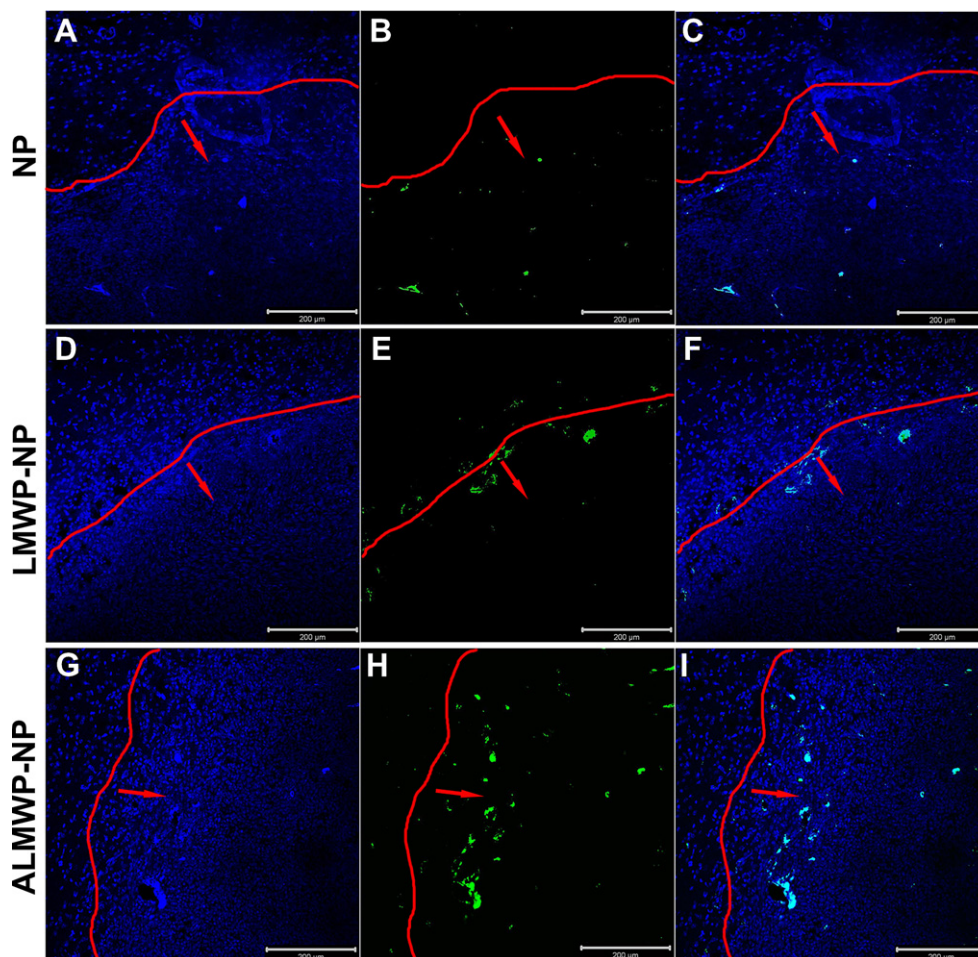
Fig. 10. Distribution of the coumarin-6-labeled NP (A–C), LMWP-NP (D–F) and ALMWP-NP (G–I) in the brain of nude mice bearing intracranial C6 glioma 3 h after i.v. administration. Image C is the combination of A and B; image F is the combination of D and E; image I is the combination of G and H. Frozen sections (20 μm of thickness) were examined under a confocal microscope. Blue: Cell nuclei. Green: Coumarin-6-labeled nanoparticles. Red lines: border of the glioma. Red arrows: direction of the glioma. Bar: 200 μm. (For interpretation of the references to colour in this figure legend, the reader is referred to the web version of this article.)
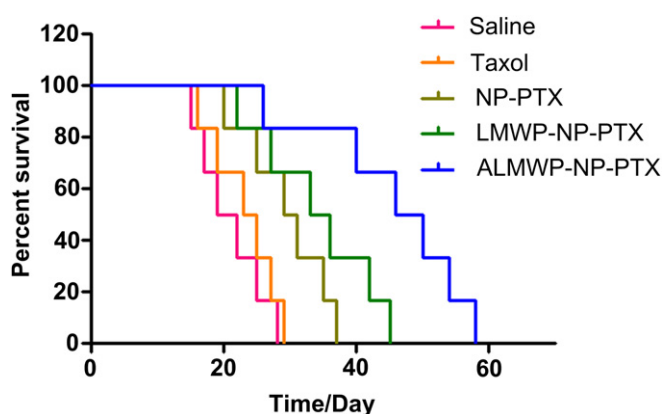
In vitro avascular C6 glioma spheroids model was established to further evaluate the tumor penetrating ability of ALMWP-NP. The tumor spheroids are free of blood vessels, therefore, transportation from cell to cell is the only way to reach the core of the tumor spheroids [51]. Confocal images showed that NP, LMWP-NP and

Fig. 11. Kaplan–Meier survival curves of mice bearing intracranial C6 glioma ($n = 6$). Mice received treatment of ALMWP-NP-PTX survived significantly longer than mice that received i.v. administrations of LMWP-NP-PTX ($p < 0.05$, log-rank analysis), NP-PTX ($p < 0.05$), Taxol® ($p < 0.01$) or saline ($p < 0.01$).

ALMWP-NP penetrated into C6 spheroids with a depth of 105.15 μm, 133.36 μm and 130.87 μm, respectively (Fig. 5). This is notable as after transporting across blood vessels. Therefore ALMWP-NP also possesses an excellent ability to penetrate deeper into the tumor to kill the glioma cells.

The improved cellular uptake led to an anticipated enhanced anti-proliferation effect. Significantly enhanced cytotoxicity was achieved for LMWP-NP-PTX and ALMWP-NP-PTX (IC_{50} 4.34 and 3.95 times lower than that of Taxol®, 3.37 and 3.07 times lower than that of NP-PTX), which we believed was contributed by the enhanced cellular association of the nanoparticles following ligand modification (Fig. 6). The improved anti-glioma efficacy of the ALMWP-NP was also confirmed *in vivo* in nude mice bearing intracranial C6 glioma (Fig. 11). The anti-glioma effect of ALMWP-NP-PTX demonstrated here was superior to that of previous studies using Aptamer-NP [33] or RGD-NP [26] to mediate PTX treatment in intracranial glioma model. The findings here offered robust evidence for the targeting therapeutic effects of ALMWP-NP-PTX, and might lead to a significant advancement in the application of CPPs for targeted therapy of glioblastoma.

5. Conclusion

We here constructed an activatable CPP termed ALMWP and conjugated it to the PEG-PCL nanoparticles aiming at enhanced

targeted glioblastoma therapy. The resulted ALMWP-NP-PTX was observed to be uniformly spherical in shape with a particle size at 121 nm and zeta potential at −21.8 ± 1.28 mV with the peptide conjugation confirmed by XPS. It also exhibited a desirable pharmacokinetic and biodistribution profile for glioblastoma-targeted drug delivery. Cellular experiments showed that ALMWP-NP exhibited significantly elevated MMP-dependent cellular accumulation in C6 cells via lipid raft-mediated endocytosis and energy-dependent macropinocytosis, and improved the cytotoxicity of PTX. *In vitro* uptake in tumor spheroid confirmed the tumor penetrating ability of ALMWP-NP, *in vivo* imaging and brain distribution justified its specific accumulation in the glioma. With these outstanding properties, ALMWP-NP-PTX showed excellent anti-glioblastoma effect in nude mice bearing intracranial C6 glioma. Our study demonstrated here opened a new avenue for treatment and experimental investigation of glioma and would encourage further studies into the application of CPPs for targeted therapy of malignant glioma.

Acknowledgments

References

[1] Kim WY, Lee HY. Brain angiogenesis in developmental and pathological processes: mechanism and therapeutic intervention in brain tumors. FEBS J 2009;276:4653—64.

[2] Ong BY, Ranganath SH, Lee LY, Lu F, Lee HS, Sahinidis NV, et al. Paclitaxel delivery from PLGA foams for controlled release in post-surgical chemotherapy against glioblastoma multiforme. Biomaterials 2009;30:3189—96.

[3] Groothuis DR. The blood-brain and blood-tumor barriers: a review of strategies for increasing drug delivery. Neuro Oncol 2000;2:45—59.

[4] Jain RK, di Tomaso E, Duda DG, Loeffler JS, Sorensen AG, Batchelor TT. Angiogenesis in brain tumours. Nat Rev Neurosci 2007;8:610—22.

[5] Liu Y, Lu WY. Recent advances in brain tumor-targeted nano-drug delivery systems. Expert Opin Drug Deliv 2012;9:671—86.

[6] Jain KK. Use of nanoparticles for drug delivery in glioblastoma multiforme. Expert Rev Neurother 2007;7:363—72.

[7] Beduneau A, Saulnier P, Benoit JP. Active targeting of brain tumors using nanocarriers. Biomaterials 2007;28:4947—67.

[8] Takara K, Hatakeyama H, Ohga N, Hida K, Harashima H. Design of a dual-ligand system using a specific ligand and cell penetrating peptide, resulting in a synergistic effect on selectivity and cellular uptake. Int J Pharm 2010;396: 143—8.

[9] Koren E, Torchilin VP. Cell-penetrating peptides: breaking through to the other side. Trends Mol Med 2012;18:385—93.

[10] Fonseca SB, Pereira MP, Kelley SO. Recent advances in the use of cell-penetrating peptides for medical and biological applications. Adv Drug Deliv Rev 2009;61:953—64.

[11] Choi YS, Lee JY, Suh JS, Kwon YM, Lee SJ, Chung JK, et al. The systemic delivery of siRNAs by a cell penetrating peptide, low molecular weight protamine. Biomaterials 2010;31:1429—43.

[12] Lee LM, Chang LC, Wrobleski S, Wakefield TW, Yang VC. Low molecular weight protamine as nontoxic heparin/low molecular weight heparin antidote (III): preliminary in vivo evaluation of efficacy and toxicity using a canine model. Aaps Pharmsci 2001;3:E19.

[13] Liang JF, Zhen L, Chang LC, Yang VC. A less toxic heparin antagonist—low molecular weight protamine. Biochemistry (Mosc) 2003;68:116—20.

[14] Tsui B, Singh VK, Liang JF, Yang VC. Reduced reactivity towards anti-protamine antibodies of a low molecular weight protamine analogue. Thromb Res 2001;101:417—20.

[15] Zhang XX, Eden HS, Chen X. Peptides in cancer nanomedicine: drug carriers, targeting ligands and protease substrates. J Control Release 2012;159:2—13.

[16] Jiang T, Olson ES, Nguyen QT, Roy M, Jennings PA, Tsien RY. Tumor imaging by means of proteolytic activation of cell-penetrating peptides. Proc Natl Acad Sci U S A 2004;101:17867—72.

[17] Aguilera TA, Olson ES, Timmers MM, Jiang T, Tsien RY. Systemic in vivo distribution of activatable cell penetrating peptides is superior to that of cell penetrating peptides. Integr Biol (Camb) 2009;1:371—81.

[18] Forsyth PA, Wong H, Laing TD, Rewcastle NB, Morris DG, Muzik H, et al. Gelatinase-A (MMP-2), gelatinase-B (MMP-9) and membrane type matrix metalloproteinase-1 (MT1-MMP) are involved in different aspects of the pathophysiology of malignant gliomas. Br J Cancer 1999;79:1828—35.

[19] Wang M, Wang T, Liu S, Yoshida D, Teramoto A. The expression of matrix metalloproteinase-2 and -9 in human gliomas of different pathological grades. Brain Tumor Pathol 2003;20:65—72.

[20] Tauro JR, Gemeinhart RA. Matrix metalloprotease triggered delivery of cancer chemotherapeutics from hydrogel matrixes. Bioconjug Chem 2005; 16:1133—9.

[21] Chau Y, Tan FE, Langer R. Synthesis and characterization of dextran-peptide-methotrexate conjugates for tumor targeting via mediation by matrix metalloproteinase II and matrix metalloproteinase IX. Bioconjug Chem 2004;15: 931—41.

[22] Olson ES, Jiang T, Aguilera TA, Nguyen QT, Ellies LG, Scadeng M, et al. Activatable cell penetrating peptides linked to nanoparticles as dual probes for in vivo fluorescence and MR imaging of proteases. Proc Natl Acad Sci U S A 2010;107:4311—6.

[23] Ke XY, Zhao BJ, Zhao X, Wang Y, Huang Y, Chen XM, et al. The therapeutic efficacy of conjugated linoleic acid — paclitaxel on glioma in the rat. Biomaterials 2010;31:5855—64.

[24] Xin HL, Jiang XY, Gu JJ, Sha XY, Chen LC, Law K, et al. Angiopep-conjugated poly(ethylene glycol)-co-poly(epsilon-caprolactone) nanoparticles as dual-targeting drug delivery system for brain glioma. Biomaterials 2011;32: 4293—305.

[25] Régina A, Demeule M, Ché C, Lavallée I, Poirier J, Gabathuler R, et al. Anti-tumour activity of ANG1005, a conjugate between paclitaxel and the new brain delivery vector Angiopep-2. Br J Pharmacol 2008;155:185—97.

[26] Zhan CY, Gu B, Xie C, Li J, Liu Y, Lu WY. Cyclic RGD conjugated poly(ethylene glycol)-co-poly(lactic acid) micelle enhances paclitaxel anti-glioblastoma effect. J Control Release 2010;143:136—42.

[27] Singla AK, Garg A, Aggarwal D. Paclitaxel and its formulations. Int J Pharm 2002;235:179—92.

[28] Xia HM, Gao XL, Gu GZ, Liu ZY, Zeng N, Hu QY, et al. Low molecular weight protamine-functionalized nanoparticles for drug delivery to the brain after intranasal administration. Biomaterials 2011;32:9888—98.

[29] Zhang W, Shi Y, Chen YZ, Ye J, Sha XY, Fang XL. Multifunctional Pluronic P123/ F127 mixed polymeric micelles loaded with paclitaxel for the treatment of multidrug resistant tumors. Biomaterials 2011;32:2894—906.

[30] Jiang XY, Sha XY, Xin HL, Chen LC, Gao XH, Wang X, et al. Self-aggregated pegylated poly (trimethylene carbonate) nanoparticles decorated with c(RGDyK) peptide for targeted paclitaxel delivery to integrin-rich tumors. Biomaterials 2011;32:9457—69.

[31] Zeng N, Hu QY, Liu ZY, Gao XL, Hu RK, Song QX, et al. Preparation and characterization of paclitaxel-loaded DSPE-PEG-liquid crystalline nanoparticles (LCNPs) for improved bioavailability. Int J Pharm 2012;424:58—66.

[32] He H, Li Y, Jia XR, Du J, Ying X, Lu WL, et al. PEGylated Poly(amidoamine) dendrimer-based dual-targeting carrier for treating brain tumors. Biomaterials 2011;32:478—87.

[33] Guo JW, Gao XL, Su LN, Xia HM, Gu GZ, Pang ZQ, et al. Aptamer-functionalized PEG-PLGA nanoparticles for enhanced anti-glioma drug delivery. Biomaterials 2011;32:8010—20.

[34] Xia HM, Gao XL, Gu GZ, Liu ZY, Hu QY, Tu YF, et al. Penetratin-functionalized PEG-PLA nanoparticles for brain drug delivery. Int J Pharm 2012;436:840—50.

[35] Mohyeldin A, Chiocca EA. Gene and viral therapy for glioblastoma: a review of clinical trials and future directions. Cancer J 2012;18:82—8.

[36] Qin Y, Chen HL, Zhang QY, Wang XX, Yuan WM, Kuai R, et al. Liposome formulated with TAT-modified cholesterol for improving brain delivery and therapeutic efficacy on brain glioma in animals. Int J Pharm 2011;420:304—12.

[37] Chen Y, Liu LH. Modern methods for delivery of drugs across the blood-brain barrier. Adv Drug Deliv Rev 2012;64:640—65.

[38] Herve F, Ghinea N, Scherrmann JM. CNS delivery via adsorptive transcytosis. AAPS J 2008;10:455—72.

[39] Chawla JS, Amiji MM. Biodegradable poly(epsilon -caprolactone) nanoparticles for tumor-targeted delivery of tamoxifen. Int J Pharm 2002;249:127—38.

[40] Hu KL, Li JW, Shen YH, Lu W, Gao XL, Zhang QZ, et al. Lactoferrin-conjugated PEG-PLA nanoparticles with improved brain delivery: in vitro and in vivo evaluations. J Control Release 2009;134:55—61.

[41] Li SD, Huang L. Pharmacokinetics and biodistribution of nanoparticles. Mol Pharm 2008;5:496—504.

[42] Chekhonin VP, Baklaushev VP, Yusubalieva GM, Pavlov KA, Ukhova OV, Gurina OI. Modeling and immunohistochemical analysis of C6 glioma in vivo. Bull Exp Biol Med 2007;143:501—9.

[43] Takahashi M, Fukami S, Iwata N, Inoue K, Itohara S, Itoh H, et al. In vivo glioma growth requires host-derived matrix metalloproteinase 2 for maintenance of angioarchitecture. Pharmacol Res 2002;46:155—63.

[44] Esteve PO, Robledo O, Potworowski EF, St-Pierre Y. Induced expression of MMP-9 in C6 glioma cells is inhibited by PDGF via a PI 3-kinase-dependent pathway. Biochem Biophys Res Commun 2002;296:864—9.

[45] Yong VW, Power C, Forsyth P, Edwards DR. Metalloproteinases in biology and pathology of the nervous system. Nat Rev Neurosci 2001;2:502—11.

[46] Funovics M, Weissleder R, Tung CH. Protease sensors for bioimaging. Anal Bioanal Chem 2003;377:956—63.

[47] Song QX, Yao L, Huang M, Hu QY, Lu Q, Wu BX, et al. Mechanisms of trans-cellular transport of wheat germ agglutinin-functionalized polymeric nano-particles in Caco-2 cells. Biomaterials 2012;33:6769—82.

[48] Gao XL, Wang T, Wu BX, Chen J, Chen JY, Yue Y, et al. Quantum dots for tracking cellular transport of lectin-functionalized nanoparticles. Biochem Biophys Res Commun 2008;377:35—40.

[49] Xin HL, Sha XY, Jiang XY, Chen LC, Law K, Gu JJ, et al. The brain targeting mechanism of Angiopep-conjugated poly(ethylene glycol)-co-poly(epsilon-caprolactone) nanoparticles. Biomaterials 2012;33:1673—81.

[50] Nam HY, Kwon SM, Chung H, Lee SY, Kwon SH, Jeon H, et al. Cellular uptake mechanism and intracellular fate of hydrophobically modified glycol chitosan nanoparticles. J Control Release 2009;135:259—67.

[51] Gao HL, Qian J, Yang Z, Pang ZQ, Xi ZJ, Cao SJ, et al. Whole-cell SELEX aptamer-functionalised poly(ethyleneglycol)-poly(epsilon-caprolactone) nanoparticles for enhanced targeted glioblastoma therapy. Biomaterials 2012;33:6264—72.